



# Observation and study of consecutive dust storms in the Taklimakan desert from March 16 to 27, 2022, using reanalysis models and lidar

Mohamed Elshora<sup>a,b,c</sup>, Haiyun Xia<sup>a,b,\*</sup>, Lian Su<sup>a</sup>, Tianwen Wei<sup>b</sup>

<sup>a</sup> School of Earth and Space Sciences, University of Science and Technology of China, Hefei 230026, China

<sup>b</sup> School of Atmospheric Physics, Nanjing University of Information Science and Technology, Nanjing 210044, China

<sup>c</sup> Department of Public Works Engineering, Faculty of Engineering, Tanta University, Tanta, 31511, Egypt

## ARTICLE INFO

### Keywords:

Taklimakan desert dust  
Dust storm  
Dust transport  
Coherent Doppler wind lidar

## ABSTRACT

A series of severe dust storms hit the Taklimakan desert between March 16 and 27, 2022, significantly deteriorating air quality throughout China. This study presents a comprehensive analysis of the vertical structure of aerosols during these dust storms, as well as their causes and impacts on China's regional and city-scale air quality, utilizing data from reanalysis models, coherent Doppler wind lidar, and air quality monitoring stations. During dust storms, intense wind layers increase dust emissions, resulting in reduced lidar detection ranges and signal strengths. In addition, lower temperatures prevail due to sunlight absorption and scattering. Moreover, high-speed winds at high altitudes increase dust particles that serve as cloud condensation nuclei, leading to increased humidity, decreased temperature, and precipitation. The Taklimakan desert's trough serves as a wind convergence zone, which promotes favorable conditions for the initiation of dust storms. Due to the steep pressure gradients, strong winds enter the Taklimakan desert through the gap between its mountains in the east, coming from northern Xinjiang and Inner Mongolia via the Hexi corridor, which facilitates the lifting and transport of dust aerosols. Dust is transported long distances from the Taklimakan desert to the eastern coasts, impacting numerous cities along the way. The emissions from these dust storms swept across most Chinese provinces. Even though each dust storm was over in the Taklimakan desert, its effects on China's air quality continued for several days. The coarse PM concentrations (PM<sub>10-2.5</sub>) in Hotan, Kashgar, Aksu, Korla, Hami, Xining, Yinchuan, Taiyuan, and Beijing spiked to levels around 14, 36, 11, 6, 7, 12, 11, 12, and 6 times higher than their 2022 averages, respectively. This study provides valuable insights into the causes and effects of the Taklimakan desert dust storms, helping authorities develop effective mitigation plans.

## 1. Introduction

Dust is one of the major aerosol species that has significant impacts on air quality, climate, visibility, and human health (Bi et al., 2022; Xu et al., 2020). Dust aerosols contribute to particulate matter concentrations and lead to air quality deterioration in the source area, and they can even travel long distances to participate in the air pollution of regional and global places (Chakravarty et al., 2021; Krasnov et al., 2014). Dust aerosols also have an impact on climate through a direct effect by absorbing and scattering sunlight that would otherwise reach the surface, causing variations in atmospheric heating and cooling, and an indirect effect by acting as cloud condensation or ice nuclei, affecting the formation of clouds and their properties and lifetime (Chen et al., 2023a; Hu et al., 2020b; Che et al., 2019; Ji et al., 2016; Choobari et al.,

2014; Huang et al., 2014). In addition, depositing dust on ice and snow reduces the surface albedo and speeds up snow melting (Qian et al., 2015). High dust concentrations have an impact on transportation and aviation safety by reducing visibility and causing hazy conditions (Jayaratne et al., 2011). Furthermore, inhaling dust particles can harm human health by entering deep into the respiratory system, resulting in a variety of respiratory and cardiovascular diseases as well as raising mortality rates (Goudie, 2014; Tam et al., 2012). Depending on visibility and wind speed, three categories of dusty weather can be identified: suspended dust, blowing dust, and dust storms. A dust storm is characterized by a strong wind that carries a considerable amount of dust, reducing visibility (Aili et al., 2021). Wu et al. (2022) and Pu and Jin (2021) demonstrated the substantial influence of surface wind, land cover, and soil moisture on the formation of dust storms. Investigating

\* Corresponding author at: School of Earth and Space Sciences, University of Science and Technology of China, Hefei 230026, China.

E-mail address: [hsia@ustc.edu.cn](mailto:hsia@ustc.edu.cn) (H. Xia).

the characteristics of dust storms is crucial for mitigating their negative influences and improving our understanding of desert dust dynamics. Dust transport, driven by large-scale atmospheric circulation and weather systems, has the potential to greatly increase air particulate matter concentrations, resulting in variable degrees of pollution over thousands to tens of thousands of kilometers (Gao et al., 2024; Victor et al., 2024).

The majority of dust emissions originate from the arid regions of Northern Africa, the Arabian Peninsula, Central Asia, and China (Castellanos et al., 2024; Merdji et al., 2023). Due to its strong winds, dry climates, and broad areas of loose sediments and sand dunes, the Taklimakan desert, located in southwestern Xinjiang in Northwest China, experiences regular dust storms. The Taklimakan desert is the

second-largest shifting sand desert in the world, with dunes varying in height from 18 to 91 m, and is a primary source of dust in East Asia (Mehta and Singh, 2018). As shown in Fig. 1, it is a portion of the Tarim Basin and is bordered to the north by the Tianshan Mountains, to the east by the Gobi Desert, to the south by the Kunlun Mountains, and to the west by the Pamir Mountains. It covers an area of 337,000 km<sup>2</sup>, making it the second-largest desert in China and the 17th-largest globally. Therefore, understanding the characteristics of the dusty weather of the Taklimakan desert is necessary. Mu et al. (2021) studied the spatio-temporal variations of dust events in the Xinjiang basin and their potential causes during 1960–2015. Zhou et al. (2023) analyzed the characteristics of Tarim basin dust weather from 1989 to 2021 and its effects on the atmospheric environment.

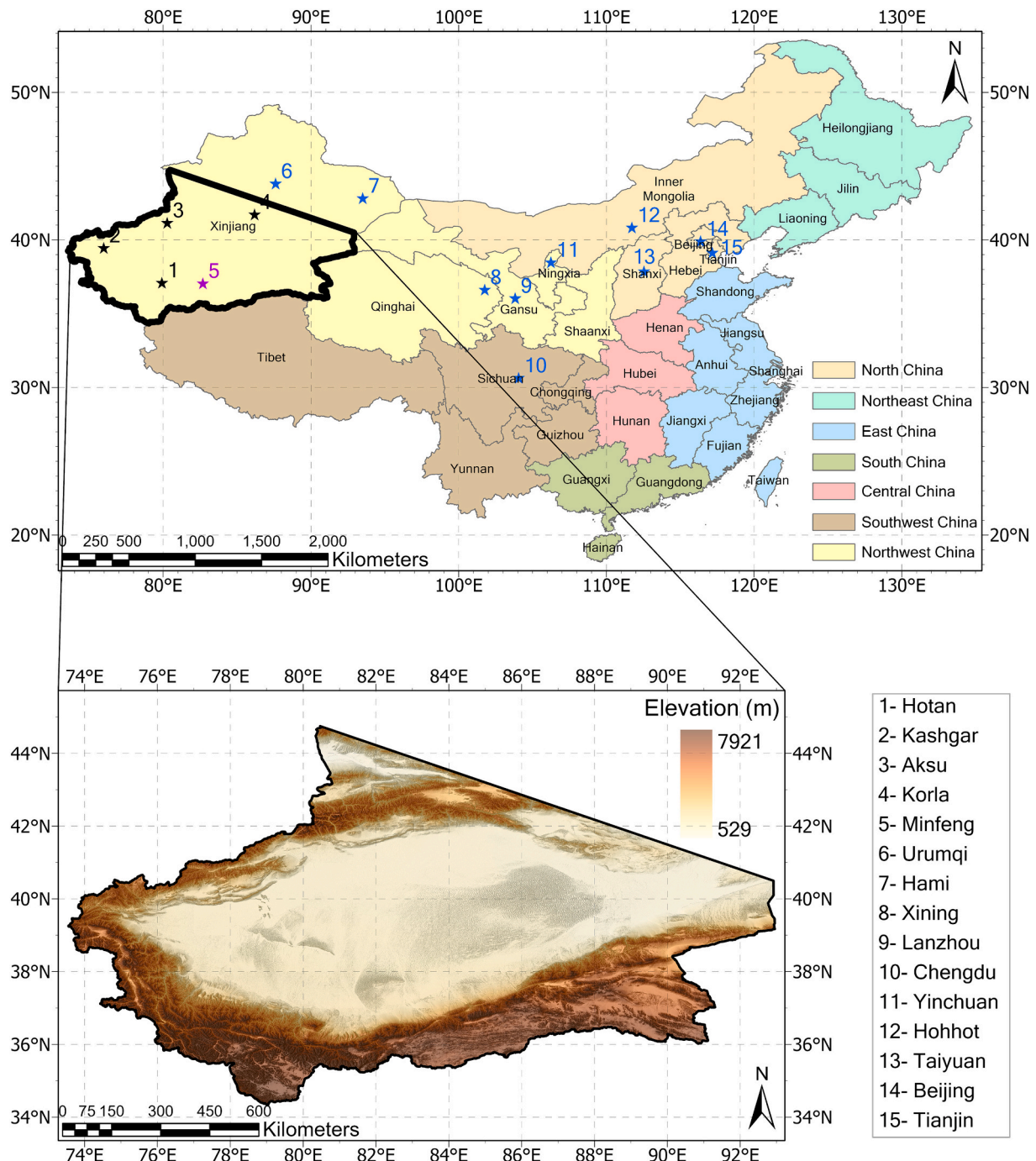


Fig. 1. The study area, including its topography and the cities used in this study.

Taklimakan desert dust particles can be raised to the upper atmosphere and transported long distances towards the east to affect the air quality of many regions (Xiong et al., 2023; Meng et al., 2020; Hu et al., 2019; Chen et al., 2017; Zhang et al., 2008). They may even travel for around 13 days to complete one full cycle around the world (Uno et al., 2009). Numerous studies have focused on how dust storms affect urban air quality. Xie et al. (2005) analyzed the concentrations of PM<sub>10</sub>, SO<sub>2</sub>, NO<sub>x</sub>, and O<sub>3</sub> during a dust storm period in Beijing. Wang et al. (2006) studied the effects of different types of dust events on PM<sub>10</sub> concentrations in different cities in northern China. Han et al. (2015) analyzed the optical properties and vertical distribution of a heavy dust event and its impact on the local air quality in Nanjing. Guan et al. (2017) investigated the variation of particulate matter concentrations due to a dust event in three cities in Gansu Province. Li et al. (2018) compared the influences of the different types of dust events on air pollutant concentrations in Hotan Prefecture. Aili et al. (2021) explored the source and transport pathways of dust storms and their contribution to air pollution in Bugur County. Tao et al. (2021) studied the effects of the transported dust aerosols on the air quality of central China. Other studies have focused on the relationships between spring dust storm frequency and meteorological conditions (Aili et al., 2016; Xiao et al., 2008; Liu et al., 2004). The mechanism of dust radiative feedback on intensifying cyclones and dust storms was also investigated (Chen et al., 2023b). In addition, the contribution of regional climate change to strengthening dust storms was studied (Hu et al., 2023). Different methods were used to study the Taklimakan desert's dust, such as aerosol optical depth products (Che et al., 2013), lidar vertical profiles (Dong et al., 2022; Hu et al., 2020a), and unmanned aerial vehicles (Zhou et al., 2022; Jin et al., 2020). Despite these valuable efforts, a single observation method could only offer a limited view of dust storms. Also, focusing on a relatively small study area limits the chance to capture the full extent of dust storm effects. Therefore, there is still a need for a comprehensive study that integrates multiple sources of data, such as reanalysis models, lidar, and ground-based monitoring stations, to thoroughly analyze the Taklimakan desert dust storms and their effects on the air quality on a national scale.

During March 16–27, 2022, a series of severe dust storms formed in the Taklimakan desert and transported dust aerosols to the eastern Pacific coastlines, deteriorating air quality throughout China. Understanding the reasons behind these dust storms and how they affect China's cities' air quality is important. Therefore, the objectives of this study are to investigate: (1) the vertical structure of aerosols during Taklimakan desert dust storms; (2) the causes of these dust storms; and (3) their effects on China's air quality on regional and city scales. This study explores the vertical distribution of aerosols during dust storms using the vertical profiles of a coherent Doppler wind lidar (CDWL), combined with dust surface mass concentrations and meteorological data from the Modern-Era Retrospective analysis for Research and Applications version 2 (MERRA-2). It also analyzes the synoptic conditions using the mean sea level pressure, wind vectors, and the geopotential height at 850 hPa from the ERA5 reanalysis dataset to investigate the reasons behind dust storms. Additionally, it investigates dust anomalies to demonstrate how dust storms affect China as a whole, as well as coarse PM concentrations to demonstrate how dust storms affect certain cities.

## 2. Material and methods

The hourly dust surface mass concentrations ( $\text{kg m}^{-3}$ ) were calculated for the area of the Taklimakan desert and the entire area of China for a period of consecutive dust storms from March 16 to 27, 2022, and they were compared temporally to each other to investigate the association between the Taklimakan desert's dust storms and their impacts on China's air quality. The dust surface mass concentrations were acquired from an hourly time-averaged 2D data collection (M2T1NXAER) in MERRA-2 at a spatial resolution of  $0.5^\circ \times 0.625^\circ$ . MERRA-2 is the

most recent satellite-era global atmospheric reanalysis conducted by NASA's Global Modelling and Assimilation Office (GMAO) utilizing the Goddard Earth Observing System Model (GEOS) version 5.12.4.

The ground-based CDWL data were retrieved from the Minfeng station ( $82.691^\circ \text{ E}$ ,  $37.068^\circ \text{ N}$ ) between March 19 and 26, 2022, to investigate the vertical dispersion of aerosols during dust storms. This lidar determines the frequency shifts to detect wind along the line of sight (LOS) (Liu et al., 2019). By using the velocity azimuth display (VAD) scanning technique, an elevation angle of  $70^\circ$  is kept constant, and the laser beam observes several positions at a yaw angle varying from  $0^\circ$  to  $360^\circ$  to form a full cone. The lidar provides 24 h of continuous observations per day, observing 1374 full cones, each with 29 to 30 LOS components and an angle of around  $12^\circ$  between each pair of positions. It has a 200-bin range, with the first 100 bins having a resolution of 30 m, the second 50 bins having a resolution of 60 m, and the third 50 bins having a resolution of 150 m. The level-1 data of this lidar is the line-of-sight wind velocity (radial velocity), carrier-to-noise ratio (CNR), and spectral width, whereas the attenuated backscatter coefficient and the wind profiles: horizontal wind speed, vertical wind speed, and wind direction, are retrieved from the level-1 data (Tang et al., 2022). In this paper, a threshold CNR of  $-18 \text{ dB}$  is used to discard the high-uncertainty data. A horizontal wind direction of  $0^\circ$  indicates wind blowing towards the north, and the direction increases clockwise. The positive values of the vertical wind speed indicate a downward direction. Additionally, The MERRA-2 dust surface mass concentrations were used to explore the effects of dust storms on Minfeng's air quality. Also, MERRA-2 meteorological data, such as air temperature ( $^\circ\text{C}$ ), specific humidity (unitless), and precipitation ( $\text{mm h}^{-1}$ ), were used to extensively investigate the vertical profiles of CDWL and study the association between meteorological variables and dust concentrations. The MERRA-2 dust surface mass concentrations and meteorological data were accessed at the Giovanni website (<https://giovanni.gsfc.nasa.gov/>).

To investigate the reasons behind these dust storms, the synoptic conditions were analyzed using meteorological variables from the ERA5 reanalysis dataset. ERA5 is the fifth-generation reanalysis of the global climate and weather produced by the European Centre for Medium-Range Weather Forecasts (ECMWF) with a spatial resolution of  $0.25^\circ \times 0.25^\circ$  and a temporal resolution of 1 h. The 10-m horizontal wind components required to calculate the speed and direction of the wind and the mean sea level pressure were accessed through the "ERA5 hourly data on single levels from 1940 to present" dataset. The geopotential at 850 hPa that was used to calculate the geopotential height was accessed through the "ERA5 hourly data on pressure levels from 1940 to present" dataset. The ERA5 meteorological data was accessed at the Copernicus climate data store website (<https://cds.climate.copernicus.eu/>).

The daily anomalies of the dust surface mass concentrations for the days between March 16 and 27 were calculated based on the annual mean of 2022 to investigate its spatial distribution and study the impacts of these dust storms on China's air quality. Although the output figures depict any variations from the norm, whether by increase or decrease, negative and weak anomalies were assigned no color to facilitate the analysis of strong anomalies associated with dust storms. The PM concentrations of four cities inside the Taklimakan desert: Hotan, Kashgar, Aksu, and Korla, during the period of these dust storms, were used to study the impacts of the Taklimakan desert's dust storms on the source area. On the other hand, the PM concentrations were accessed for cities outside the Taklimakan desert: Urumqi, Hami, Xining, Lanzhou, Chengdu, Yinchuan, Hohhot, Taiyuan, Beijing, and Tianjin, to analyze the impacts of the transported dust on distant urban cities. The hourly concentrations of PM<sub>2.5</sub> and PM<sub>10</sub> were accessed through the China National Environmental Monitoring Centre (<http://www.cnemc.cn>).

### 3. Results and discussion

#### 3.1. Dust storms of the Taklimakan desert

In the spring of 2022, a period of consecutive dust storms was observed in the Taklimakan desert. It began on March 16 with a weak storm, progressed to strong storms on March 19 and 20, and ended on March 24 with other strong storms. These dust storms and their impacts on the air quality in China should be studied. Fig. 2 shows the temporal distribution of the hourly dust surface mass concentrations averaged for the Taklimakan desert area and the entire area of China from March 16 to 27, 2022. The first dust event lasted for 25 h (from the start of the climb to the end of the drop in the dust concentrations of the Taklimakan desert) and recorded its peak at 16:30 on March 16, with dust concentrations of  $0.75 \times 10^{-6} \text{ kg m}^{-3}$  for the Taklimakan desert and  $0.89 \times 10^{-7} \text{ kg m}^{-3}$  for China. The second dust event lasted for 119 h and recorded its peak at 17:30 on March 19, with dust concentrations of  $1.60 \times 10^{-6} \text{ kg m}^{-3}$  for the Taklimakan desert and  $1.63 \times 10^{-7} \text{ kg m}^{-3}$  for China. The third dust event lasted for 97 h and recorded its peak at 16:30 on March 24, with dust concentrations of  $1.38 \times 10^{-6} \text{ kg m}^{-3}$  for the Taklimakan desert and  $1.58 \times 10^{-7} \text{ kg m}^{-3}$  for China. The high association between the temporal distribution of dust concentrations in the Taklimakan desert and that of China demonstrates that dust events in the Taklimakan desert have a significant impact on China's air quality. Additionally, it is noted that the vertical distance between the Taklimakan Desert's curve and China's curve is small during the dust event and large after its end. This pattern suggests that even though the Taklimakan desert dust storm is over, its effects on China's air quality continue for several days. This dust event was chosen to be investigated because it had the strongest dust storm in spring, occurring on March 19, and it consisted of three successive dust storms in a short period, causing overlapping influences on China's air quality. The mean dust concentration over the Taklimakan desert during these dust storms was  $0.62 \times 10^{-6} \text{ kg m}^{-3}$ , with a difference of  $0.29 \times 10^{-6} \text{ kg m}^{-3}$  from the 2022 mean dust concentration, which indicates severe dust storms. These dust storms had a substantial impact on the air quality of China, with the

country's mean dust concentration of  $0.90 \times 10^{-7} \text{ kg m}^{-3}$ , which was  $0.35 \times 10^{-7} \text{ kg m}^{-3}$  more than that of 2022.

#### 3.2. Vertical distribution of aerosols during dust storms

Dust storms are common in the southern parts of the Taklimakan desert (Jin et al., 2024). Minfeng City was found to have a higher frequency of blowing dust events, according to the findings of Yang et al. (2016). As a result, the vertical profiles of Minfeng's CDWL were utilized to investigate the vertical dispersion of aerosols during dust storms. The MERRA-2 dust surface mass concentrations ( $\text{kg m}^{-3}$ ) were also used to show the effects of dust storms on Minfeng's air quality. In addition, meteorological data from the MERRA-2 model, such as air temperature ( $^{\circ}\text{C}$ ), specific humidity (unitless), and precipitation ( $\text{mm h}^{-1}$ ), were used to extensively examine the vertical profiles of CDWL and to explore the association between meteorology and dust concentrations. Fig. 3 shows the vertical profiles of CDWL in Minfeng between March 19 and 26, 2022, as well as the temporal distribution of MERRA-2 dust surface mass concentrations, air temperature, specific humidity, and precipitation. Two periods of high dust concentrations, including four peaks, were observed during the period of dust storms.

A southern horizontal wind speed of  $5\text{--}10 \text{ m s}^{-1}$  was observed at an altitude of 2 km at 00:00 on March 19. The lidar detection range at that time was 3 km, showing a difference in wind direction between this layer (southerly wind) and the near-to-surface layer (northerly wind). Around 11:00, this southern wind layer proceeded downward with an increasing speed, reaching  $14 \text{ m s}^{-1}$ , and covering a height of 0.5–1.5 km, producing dust activity and limiting the lidar detection range to 2.2 km. These dust activities accelerated after the high-speed wind layer arrived at the surface at 15:00 with a speed of  $5\text{--}10 \text{ m s}^{-1}$  and changed its direction to be northerly. This was accompanied by the beginning of an increase in dust concentrations, which reached a peak of  $1.61 \times 10^{-6} \text{ kg m}^{-3}$  at 4:00 on March 20 when this high-speed wind layer was about to end, leading to a lower detection range of around 1 km. At 17:00 on March 20, the surface experienced a northern high-speed wind layer with a speed of  $5\text{--}12 \text{ m s}^{-1}$ , which increased dust concentrations again

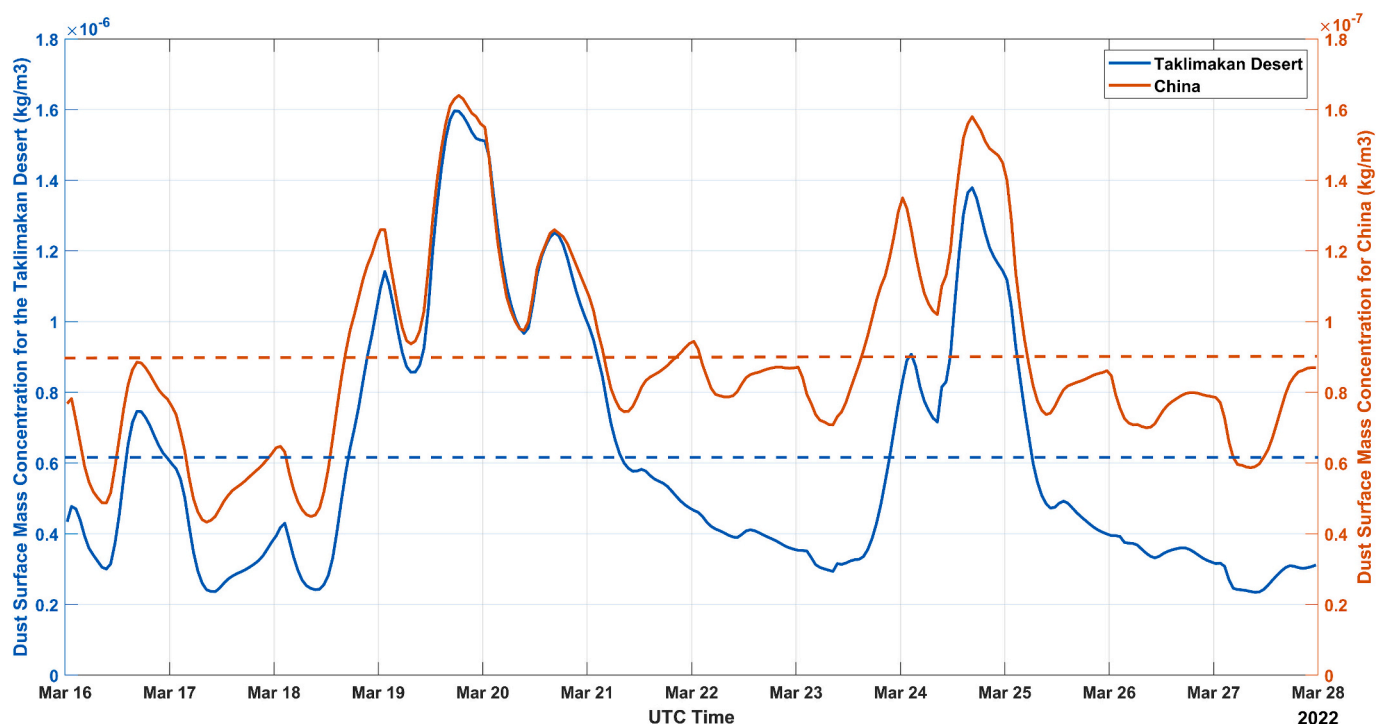
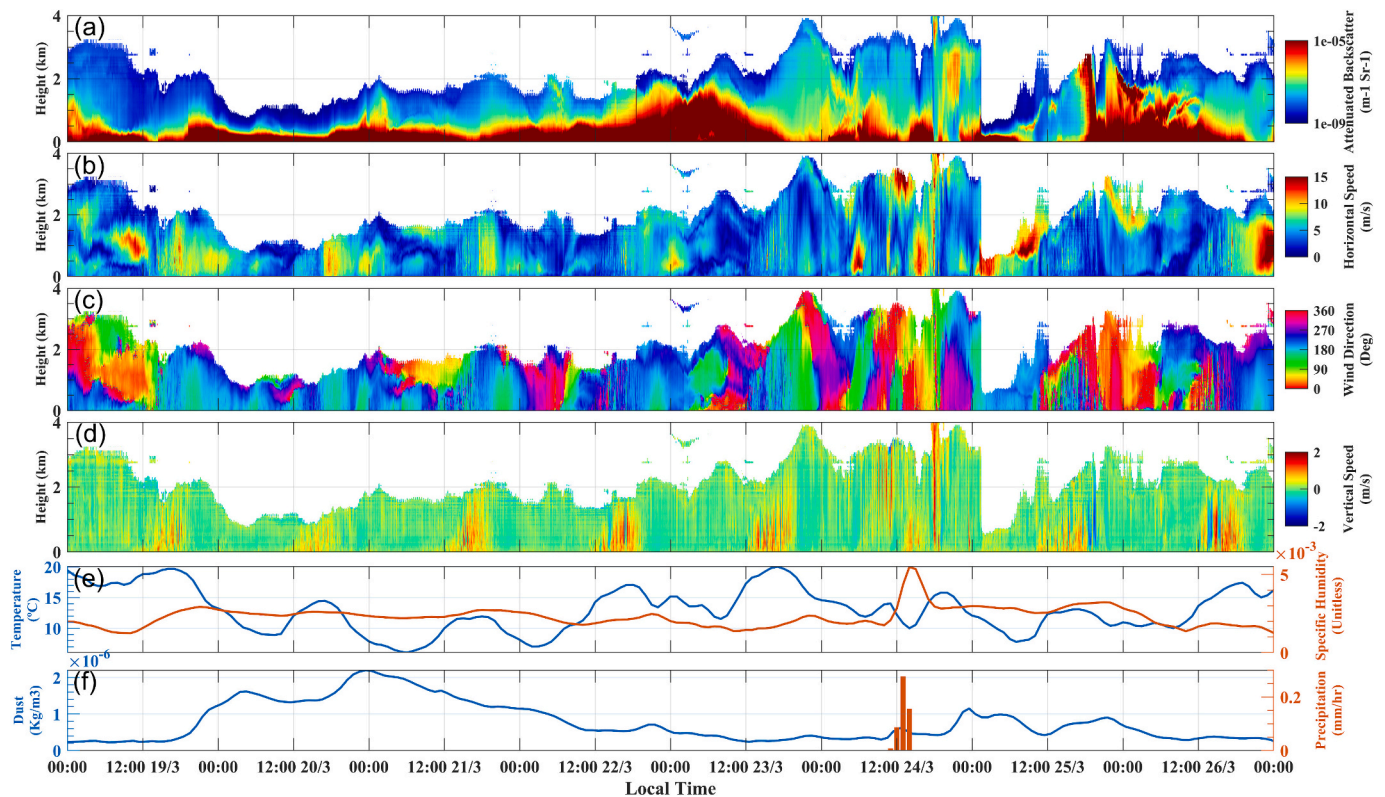


Fig. 2. The temporal distribution of the hourly dust surface mass concentrations averaged for the Taklimakan desert area and the entire area of China from March 16 to 27, 2022, the dashed lines represent the mean levels of dust during the dust event period



**Fig. 3.** The vertical profiles of CDWL: (a) Attenuated Backscatter Coefficient; (b) Horizontal Wind Speed; (c) Wind Direction; and (d) Vertical Speed, along with the temporal distribution of the MERRA-2: (e) air temperature; specific humidity; (f) dust surface mass concentrations; and precipitation in Minfeng during March 19–26, 2022

to a peak of  $2.20 \times 10^{-6} \text{ kg m}^{-3}$  at 0:00 on March 21 with the disappearance of this high-speed wind layer. After that, the dust concentrations started to decrease gradually, and the lidar detection range increased again to around 2 km. With the end of this dust storm at 18:30 on March 22, the lidar lens was cleaned of the accumulated dust that attenuated and scattered the laser light, which led to intensified signal strength. A broader range of higher attenuated backscatter coefficients was also detected after cleaning the lens, which reveals the relationship between signal strength and backscattering at higher altitudes. It was found that temperatures decreased during this dust storm; the maximum temperature on March 20 and 21 was  $14.47 \text{ }^\circ\text{C}$  and  $11.93 \text{ }^\circ\text{C}$ , respectively, compared to  $19.68 \text{ }^\circ\text{C}$  on March 19. This may be attributed to the fact that suspended dust absorbs or scatters sunlight and blocks some of the solar radiation that would otherwise reach the surface, resulting in reduced temperatures (Kok et al., 2023).

After the first dust storm's effects subsided, the dust concentration decreased to its lowest level of  $2.38 \times 10^{-7} \text{ kg m}^{-3}$  at 12:00 on March 23. This was associated with lower backscattering values at the surface layer and an extended detection range of about 4 km at 22:00 on March 23, as well as an increase in the day's maximum temperature to  $20.03 \text{ }^\circ\text{C}$ . Between 4:30 and 6:30 on March 24, a northwestern horizontal wind speed of  $10\text{--}15 \text{ m s}^{-1}$  was observed on the surface to an altitude of 1.5 km. After that, it was seen at a height of 3 km at 8:30 before changing its direction to be southerly and increasing its speed to a maximum of  $18 \text{ m s}^{-1}$  after 12:00. This high-speed wind layer at a height of around 3 km can increase dust particles that serve as cloud condensation nuclei, facilitating cloud droplet production (Karydis et al., 2011). The clouds formed by dust particles may lead to an increase in humidity, a decrease in temperature, and precipitation. This was evident at 14:00 on March 24, when the specific humidity climbed to  $5.48 \times 10^{-3}$  and the temperature dropped to  $10 \text{ }^\circ\text{C}$ , in addition to falling rains between 12:00 and 14:00 with a maximum rate of  $0.28 \text{ mm h}^{-1}$ . This

wind layer moved downward at 14:00 with a speed of  $5\text{--}15 \text{ m s}^{-1}$  and covered the height from the surface to an altitude of about 2 km, causing the beginning of an increase in dust concentrations at 18:00. With an additional impact from another southeastern wind layer with a maximum speed of  $9 \text{ m s}^{-1}$  around 22:30, the dust concentration reached its peak of  $1.15 \times 10^{-6} \text{ kg m}^{-3}$  at about 0:00 on March 25, and the lidar detection range decreased to around 0.5 km at 1:30. After that, a northeastern wind layer with a speed of  $10\text{--}17 \text{ m s}^{-1}$  started to hit the surface at 1:30 on March 25 before it moved upward at 6:00 to cover a height between 0.5 and 1.7 km, leading to another increase in the dust concentrations, which peaked again at  $9.02 \times 10^{-7} \text{ kg m}^{-3}$  at 21:00. The impacts of this dust storm disappeared at 10:00 on March 26, when the dust concentration reached its lowest value of  $2.86 \times 10^{-7} \text{ kg m}^{-3}$ . The maximum temperature on March 25 dropped to  $13.1 \text{ }^\circ\text{C}$ , which may be linked to the dust storm particles blocking some of the solar radiation from reaching the surface.

### 3.3. Synoptic conditions

Fig. 4a–c and Fig. 4d–f show the mean sea level pressure (hPa), geopotential height at 850 hPa (m), and 10-m horizontal wind ( $\text{m s}^{-1}$ ) of the March 19 and March 24 dust events, respectively. The conditions of each dust event were analyzed three times: at its start, throughout its increase, and at its peak. Regarding the March 19 dust event, high-pressure systems covered wide areas in the north, such as eastern Kazakhstan, southern Russia, eastern Mongolia, northern Xinjiang, and Inner Mongolia, and expanded with time to include Northeast China and parts of East and Central China. A trough with a pressure of roughly 995 hPa was found in the Taklimakan desert, indicating an ideal environment for dust storm formation (Cao and Chen, 2022) (Fig. 4a). As a result of these severe pressure gradients, strong winds got into the Taklimakan desert through the gap between its mountains in the east,

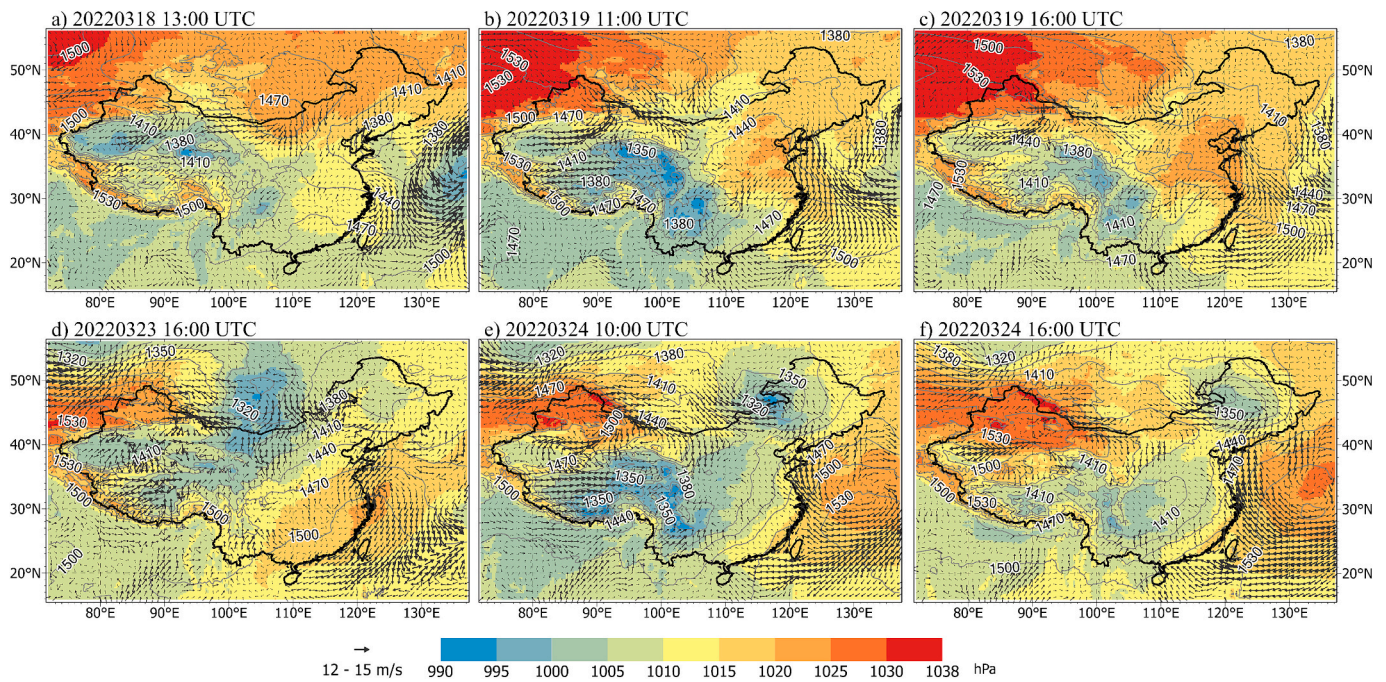


**Fig. 4.** The mean sea level pressure (hPa, shading) overlapped by geopotential height at 850 hPa (m, contours) and 10-m horizontal wind ( $\text{m s}^{-1}$ , vectors) at (a) 13:00 UTC on March 18; (b) 11:00 UTC on March 19; (c) 16:00 UTC on March 19; (d) 16:00 UTC on March 23; (e) 10:00 UTC on March 24; (f) 16:00 UTC on March 24

coming from northern Xinjiang and Inner Mongolia via the Hexi corridor. The movement of the high-pressure system to cover a large region in the north in relation to the Taklimakan desert with a pressure of around 1035 hPa increased the speeds of the wind that entered the Taklimakan desert, which facilitated the lifting and transport of dust aerosols (Fig. 4b and Fig. 4c). It is well known that strong wind is one of the necessary conditions for dust uplift (Yu et al., 2023; Sun et al., 2022; Liu et al., 2020). A low-pressure center with a counterclockwise cyclone was observed at  $137^\circ \text{E}$ ,  $33^\circ \text{N}$  (Fig. 4a). In the northern hemisphere, a low-pressure system rotates counterclockwise, whereas a high-pressure system rotates clockwise (Filonchik, 2022). In addition, a low-pressure system in areas in Northwest and Southwest China, which reached a pressure of around 990 hPa, received strong winds from the Gobi Desert, the Tibetan plateau, and East China (Fig. 4b). The sharp variations in geopotential height in the southern and western borders of the Tibetan plateau may be responsible for the atmospheric disturbances that result in high wind speeds originating from the plateau.

Regarding the March 24 dust event, high-pressure systems were observed in northern Xinjiang and eastern Kazakhstan, as well as in East and South China and the Pacific Ocean. The Taklimakan desert's trough, which had a pressure of around 1000 hPa and lower geopotential heights, acted as a wind convergence zone, where winds arrived from diverse directions, supporting the favorable conditions for the initiation of a dust storm (Fig. 4d). Broomandi et al. (2023) also confirmed the convergence of winds over the Taklimakan desert during a study of a major dust storm event across Central Asia on November 3–4, 2021. The migration of the high-pressure system towards the east to include areas in Mongolia and Inner Mongolia increased the pressure gradients and caused strong winds that got into the Taklimakan desert through the gap between its mountains (Fig. 4e and Fig. 4f). A counterclockwise cyclone originated in a low-pressure region in Mongolia, with a center around  $105^\circ \text{E}$ ,  $49^\circ \text{N}$  (Fig. 4d); after that, it moved eastward to reach North China at around  $117^\circ \text{E}$ ,  $47^\circ \text{N}$ , and  $119^\circ \text{E}$ ,  $48^\circ \text{N}$  (Fig. 4e and Fig. 4f, respectively). Furthermore, steep pressure gradients affected the low-pressure area in Northwest and Southwest China with strong winds from the Tibetan plateau and the Gobi Desert (Fig. 4e). Finally, strong surface winds, a low-pressure system, and lower geopotential heights in

the Taklimakan desert all suggest a higher probability of dust storm development in this area.

#### 3.4. Effects of dust storms on China's air quality

To study the effects of the dust storms that occurred in the Taklimakan desert from March 16 to 27, 2022, on China's air quality, the spatial distribution of daily dust surface mass concentration anomalies from March 16 to 27 was investigated, as shown in Fig. 5. The dust anomalies were derived by subtracting the 2022 mean dust concentrations from the daily averages from March 16 to 27. As a result, this figure depicts any deviations from the norm, whether by increase or decrease. Negative anomalies and weak anomalies (smaller than  $0.025 \times 10^{-6} \text{ kg m}^{-3}$ ) were assigned no color to facilitate the analysis of strong anomalies associated with dust storms. To analyze the impact of these dust storms on the air quality of Chinese cities, the coarse PM concentrations ( $\text{PM}_{10-2.5}$ ) were calculated for cities inside (Hotan, Kashgar, Aksu, and Korla) and outside (Urumqi, Hami, Xining, Lanzhou, Chengdu, Yinchuan, Hohhot, Taiyuan, Beijing, and Tianjin) the Taklimakan desert, covering different places from west to east, for the period of these dust storms. Therefore, Fig. 6 shows the temporal distribution of the hourly  $\text{PM}_{10-2.5}$  concentrations for cities inside and outside the Taklimakan desert from March 16 to 27, 2022. On March 16, a weak dust storm with a maximum anomaly value of  $1.43 \times 10^{-6} \text{ kg m}^{-3}$  formed in the Taklimakan desert, covering a small area, and it was accompanied by a rise in dust concentrations in the Gobi Desert region in western Inner Mongolia. In addition, there were no areas across China and Mongolia affected by earlier dust events. This dust storm rapidly dissipated on March 17 before dispersing to various places in Xinjiang, Qinghai, and Gansu, with the maximum anomaly value of  $0.60 \times 10^{-6} \text{ kg m}^{-3}$  found in the northern parts of the Taklimakan desert.

This dust storm impacted cities inside the Taklimakan desert, including Aksu, in which coarse PM concentrations began increasing at 23:00 on March 16 to reach a peak of  $1238 \mu\text{g m}^{-3}$  at 18:00 on March 17, and Korla, in which coarse PM concentrations began increasing at 2:00 on March 17 and peaked at  $524 \mu\text{g m}^{-3}$  at 12:00 on March 17. In addition, it affected the coarse PM concentrations of cities outside the

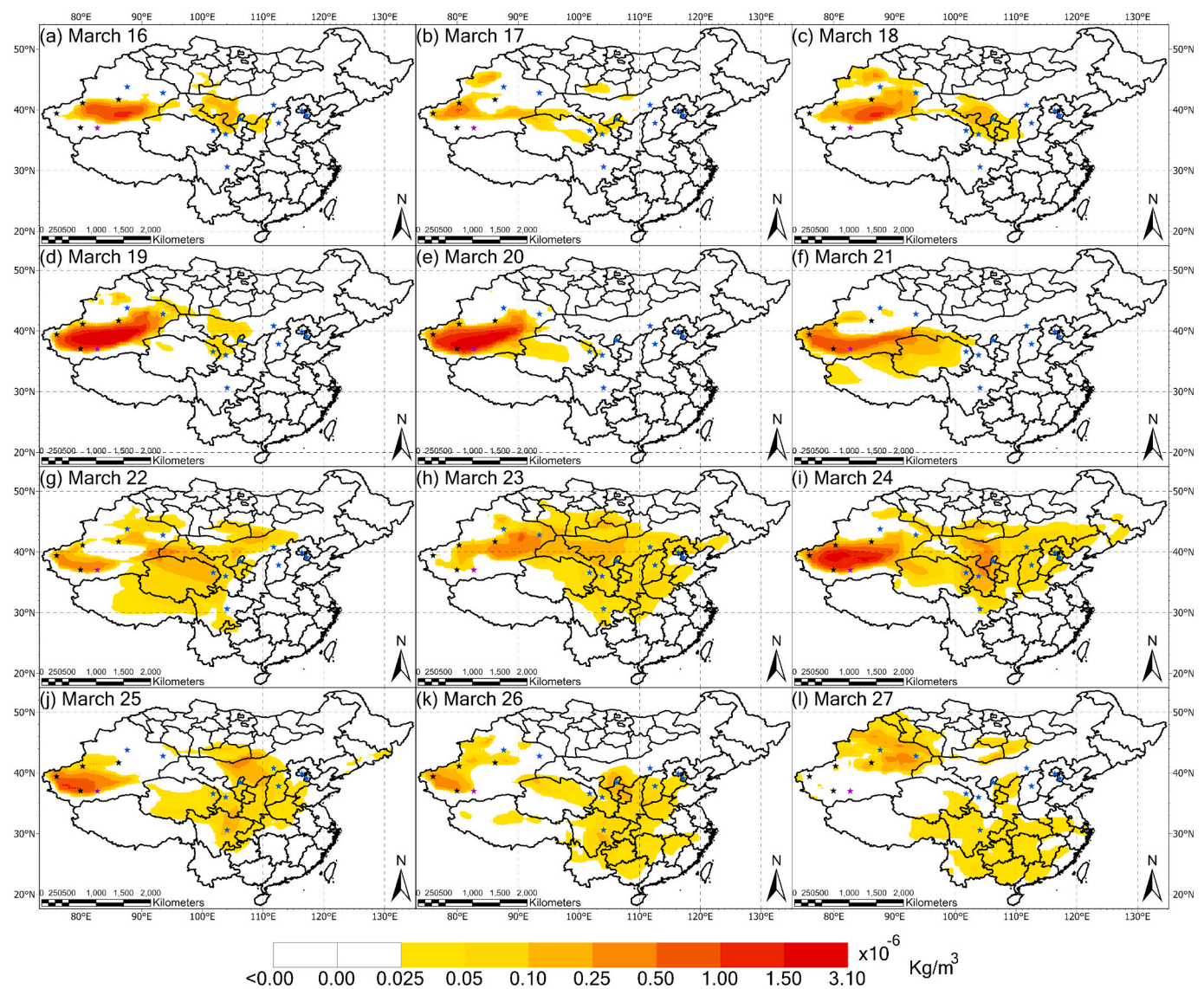


Fig. 5. The spatial distribution of the daily dust surface mass concentration anomalies from March 16 to 27, 2022.

Taklimakan desert, such as Xining (a peak of  $307 \mu\text{g m}^{-3}$  at 13:00 on March 17), Lanzhou (a peak of  $401 \mu\text{g m}^{-3}$  at 00:00 on March 17), and Yinchuan (a peak of  $411 \mu\text{g m}^{-3}$  at 17:00 on March 16).

On March 18, the Taklimakan desert witnessed the formation of another dust storm with a maximum anomaly value of  $1.36 \times 10^{-6} \text{ kg m}^{-3}$ , with an increase in dust emissions across eastern and northern Xinjiang, western Inner Mongolia, Ningxia, and parts of Gansu and Shaanxi. This dust storm peaked on March 19 and covered the whole Taklimakan desert with a maximum anomaly value of  $3.09 \times 10^{-6} \text{ kg m}^{-3}$ , coinciding with a reduction in dust concentrations in the Gobi Desert area. On March 20, the maximum anomaly value in the Taklimakan desert dropped to  $2.07 \times 10^{-6} \text{ kg m}^{-3}$ , indicating that the dust storm started to subside. However, large quantities of dust were lifted into the air and could be transported by the wind. It is evident that the region with the large dust concentrations extended to include southern Xinjiang and began to migrate east, affecting western Qinghai. It is also clear that the Gobi Desert stopped emitting high concentrations of dust, implying that the next consequences would be the result of the dust storm generated in the Taklimakan desert. On March 21, the intensity of this dust storm and its covered area in the Taklimakan desert continued to decrease, and the maximum anomaly value decreased to  $1.05 \times 10^{-6} \text{ kg m}^{-3}$ . Nevertheless, the extent of the high dust concentrations

stretched to the east, including all of Qinghai and portions of Tibet. With the dust storm coming to an end on March 22, covering a small area in the Taklimakan desert with a maximum anomaly value of  $0.45 \times 10^{-6} \text{ kg m}^{-3}$ , the area of the high dust concentrations continued to expand to cover parts of Xinjiang, Sichuan, Gansu, Ningxia, Inner Mongolia, and southern Mongolia. The dust storm in the Taklimakan desert totally disappeared on March 23. Also, the winds proceeded to transfer dust aerosols eastward, affecting additional places such as Shaanxi, Shanxi, Hubei, Henan, Shandong, Hebei, Beijing, and Liaoning, with a maximum anomaly value of  $0.71 \times 10^{-6} \text{ kg m}^{-3}$ .

Cities inside the Taklimakan desert were affected by this dust storm, such as Hotan, which had a progressive increase in coarse PM concentrations beginning at 00:00 on March 18 and lasting until March 23, recording a peak of  $3195 \mu\text{g m}^{-3}$  at 15:00 on March 20, and Korla, in which the coarse PM concentrations had three peaks at 6:00 on March 18, 11:00 on March 22, and 10:00 on March 23 with an average of  $353 \mu\text{g m}^{-3}$ . Moreover, cities outside the Taklimakan desert witnessed an increase in their coarse PM concentrations, such as Urumqi (two peaks at 21:00 on March 21 and 16:00 on March 22 with an average of  $45 \mu\text{g m}^{-3}$ ), Hami (four peaks at 6:00 on March 19, 5:00 on March 20, 8:00 on March 21, and 19:00 on March 23 with an average of  $298 \mu\text{g m}^{-3}$ ), and Xining (three peaks at 7:00 on March 18, 10:00 on March 19 and 7:00 on

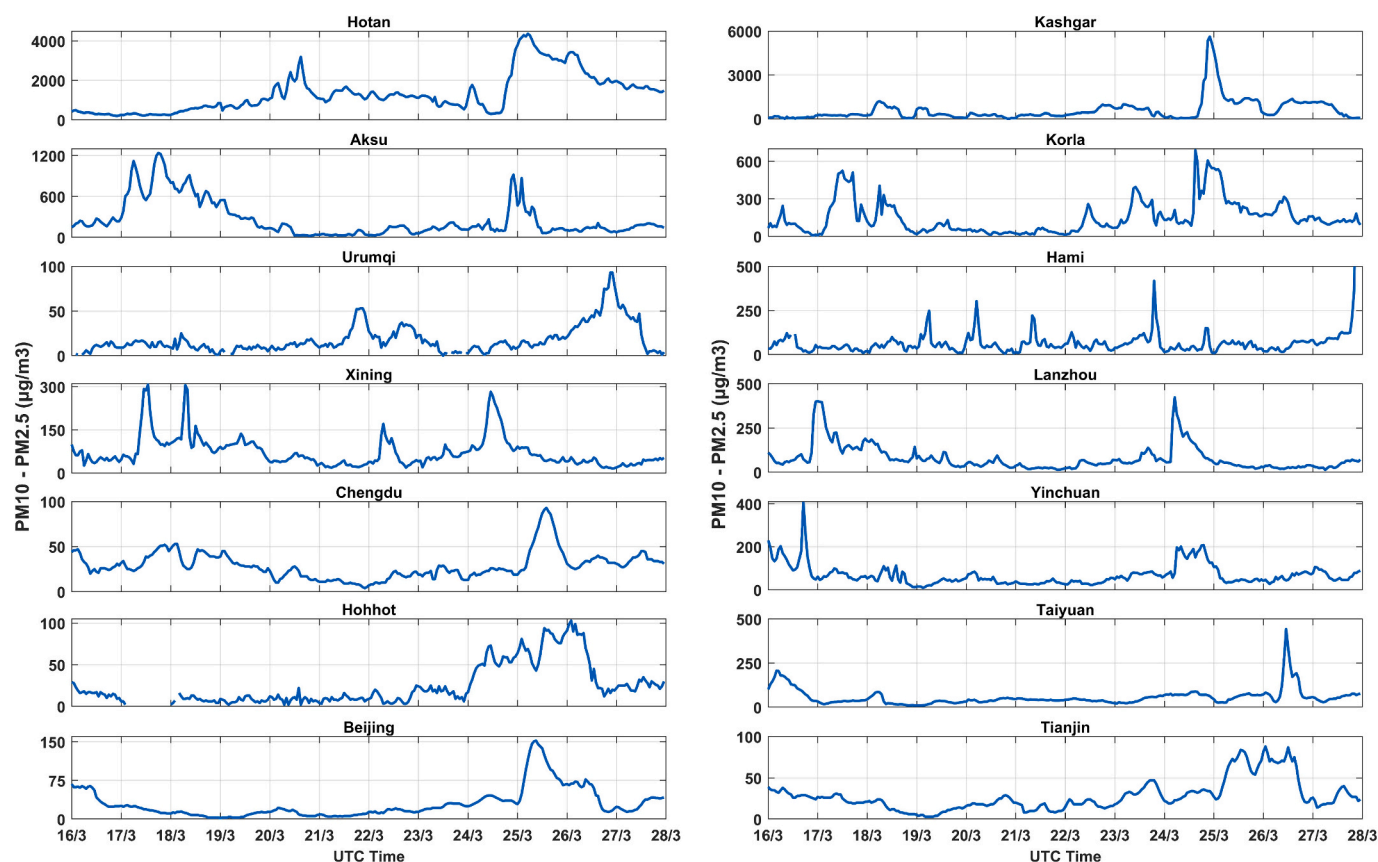


Fig. 6. The temporal distribution of the hourly  $PM_{10-2.5}$  concentrations for cities inside and outside the Taklimakan desert from March 16 to 27, 2022.

March 22 with an average of  $204 \mu\text{g m}^{-3}$ ).

During the spread of dust aerosols across China, another dust storm was recorded on March 24 in the Taklimakan desert, with a maximum anomaly value of  $1.72 \times 10^{-6} \text{ kg m}^{-3}$ . On March 25, the intensity of the new dust storm dropped as it moved into western Xinjiang, where its maximum anomaly value decreased to  $1.16 \times 10^{-6} \text{ kg m}^{-3}$ , simultaneously with a decrease in the high dust concentration area of the previous storm. On March 26, the intensity of the new dust storm continued to decrease, with a small area in western Xinjiang recording a maximum anomaly value of  $0.51 \times 10^{-6} \text{ kg m}^{-3}$ . Furthermore, the previous dust storm's impact area moved southward, excluding some places in Mongolia and Inner Mongolia, and including some other places in Jiangxi, Hunan, and Guangxi. On March 27, some additional places were excluded from the previous dust storm's impact area, such as Gansu, Ningxia, Hebei, Shanxi, and Henan. Also, the new dust storm in the Taklimakan desert completely disappeared, after the movement of its remaining effects into northern Xinjiang, recording a maximum anomaly value of  $0.50 \times 10^{-6} \text{ kg m}^{-3}$ .

The new dust storm significantly affected the coarse PM concentrations of all cities inside the Taklimakan desert: Hotan (a peak of  $4367 \mu\text{g m}^{-3}$  at 5:00 on March 25), Kashgar (a peak of  $5623 \mu\text{g m}^{-3}$  at 22:00 on March 24), Aksu (a peak of  $919 \mu\text{g m}^{-3}$  at 22:00 on March 24), and Korla (a peak of  $687 \mu\text{g m}^{-3}$  at 15:00 on March 24). The influences of the previous dust storm lasted after March 24 to affect cities such as Urumqi (a peak of  $93 \mu\text{g m}^{-3}$  at 21:00 on March 26), Xining (a peak of  $282 \mu\text{g m}^{-3}$  at 11:00 on March 24), Lanzhou (a peak of  $423 \mu\text{g m}^{-3}$  at 5:00 on March 24), Chengdu (a peak of  $93 \mu\text{g m}^{-3}$  at 14:00 on March 25), Yinchuan (several peaks throughout March 24 with an average of  $201 \mu\text{g m}^{-3}$ ), Hohhot (several peaks throughout March 24, 25, and 26 with an average of  $87 \mu\text{g m}^{-3}$ ), Taiyuan (a peak of  $443 \mu\text{g m}^{-3}$  at 11:00 on March 26), Beijing (a peak of  $152 \mu\text{g m}^{-3}$  at 9:00 on March 25), and Tianjin (several peaks throughout March 25 and 26 with an average of  $86 \mu\text{g m}^{-3}$ ).

$\text{m}^{-3}$ ).

#### 4. Conclusion

This study investigated consecutive dust storms in the Taklimakan desert on March 16–27, 2022, that affected the air quality in most areas of China. The vertical distribution of aerosols during these dust storms was analyzed using the vertical profiles of a coherent Doppler wind lidar. During dust storms, strong wind layers are detected, as well as a decreased lidar detection range and signal intensity due to accumulated dust. Also, lower temperatures are recorded as a result of blocking portions of solar radiation from reaching the surface. Furthermore, a high-altitude wind layer may increase dust aerosols that serve as cloud condensation nuclei, causing increased humidity, decreased temperature, and precipitation. The reasons behind these dust storms were explored using the mean sea level pressure, wind, and geopotential height from the ERA5 reanalysis dataset. The existence of a trough in the Taklimakan desert with lower geopotential heights and pressure around 995 hPa, along with the convergence of winds from several directions, provided an ideal environment for the initiation of dust storms. The steep pressure gradients between high-pressure systems in the north, such as in eastern Kazakhstan, northern Xinjiang, Mongolia, and Inner Mongolia, and the low-pressure system in the Taklimakan desert generated strong winds that penetrated the gap between its mountains, facilitating the development and intensification of these dust storms. The effects of these dust storms on China's air quality were investigated on a regional scale using MERRA-2 dust surface mass concentrations and on a city scale using coarse PM concentrations. It was demonstrated that the Taklimakan desert is the primary source of dust in China, and its dust storms affect many regions, such as Xinjiang, Gansu, Ningxia, Shaanxi, Shanxi, southern parts of Mongolia, western parts of Inner Mongolia, and northern parts of Qinghai. It was confirmed that dust is transported

long distances from the west to urban cities such as Beijing in the east, affecting the air quality of numerous cities along the way. Even if the dust storm is over in the Taklimakan desert, its impacts on China's air quality last for several days. To conclude, the integration of numerous data sources could offer a comprehensive picture of the causes, effects, and vertical structure of the Taklimakan desert dust storms.

### CRedit authorship contribution statement

**Mohamed Elshora:** Writing – review & editing, Writing – original draft, Visualization, Methodology, Investigation, Formal analysis, Data curation. **Haiyun Xia:** Writing – review & editing, Writing – original draft, Validation, Supervision, Methodology, Investigation, Formal analysis, Data curation, Conceptualization. **Lian Su:** Software, Resources, Investigation, Formal analysis, Data curation. **Tianwen Wei:** Software, Resources, Data curation.

### Declaration of competing interest

The authors declare no competing interests.

### Data availability

The ERA5 meteorological data is freely available at the Copernicus climate data store website (<https://cds.climate.copernicus.eu/>). The Giovanni website (<https://giovanni.gsfc.nasa.gov/>) provides free access to the MERRA-2 dust surface mass concentrations and meteorological variables. The hourly concentrations of PM<sub>2.5</sub> and PM<sub>10</sub> are accessed through the China National Environmental Monitoring Centre (<http://www.cnemc.cn>).

### References

- Aili, A., Kim Oanh, N., Abuduwaili, J., 2016. Variation Trends of Dust Storms in Relation to Meteorological Conditions and Anthropogenic Impacts in the Northeast Edge of the Taklimakan Desert, China. *Open J. Air Pollut.* 5, 127–143. <https://doi.org/10.4236/ojap.2016.54010>.
- Aili, A., Xu, H., Kasim, T., Abulikemu, A., 2021. Origin and Transport Pathway of Dust storm and its Contribution to Particulate Air Pollution in Northeast Edge of Taklimakan Desert, China. *Atmosphere* 12, 113. <https://doi.org/10.3390/atmos12010113>.
- Bi, J., Li, Z., Zuo, D., Yang, F., Li, B., Ma, J., Huang, Z., He, Q., 2022. Dust Aerosol Vertical Profiles in the Hinterland of Taklimakan Desert during Summer 2019. *Front. Environ. Sci.* 10, 851915. <https://doi.org/10.3389/fenvs.2022.851915>.
- Broomandi, P., Mohammadpour, K., Kaskaoutis, D.G., Fathian, A., Abdullaev, S.F., Maslov, V.A., Nikfal, A., Jahanbakhshi, A., Aubakirova, B., Kim, J.R., Satyanaga, A., Rashki, A., Middleton, N., 2023. A Synoptic- and Remote Sensing-based Analysis of a Severe Dust storm event over Central Asia. *Aerosol Air Qual. Res.* 23 <https://doi.org/10.4209/aaqr.220309>.
- Cao, J., Chen, S., 2022. The Tibetan Plateau as dust aerosol transit station in middle troposphere over northern East Asia: a case study. *Atmos. Res.* 280, 106416. <https://doi.org/10.1016/j.atmosres.2022.106416>.
- Castellanos, P., Colarco, P., Espinosa, W.R., Guzewich, S.D., Levy, R.C., Miller, R.L., Chin, M., Kahn, R.A., Kemppinen, O., Moosmüller, H., Nowottnick, E.P., Rocha-Lima, A., Smith, M.D., Yorks, J.E., Yu, H., 2024. Mineral dust optical properties for remote sensing and global modeling: a review. *Remote Sens. Environ.* 303, 113982. <https://doi.org/10.1016/j.rse.2023.113982>.
- Chakravarty, K., Vincent, V., Vellore, R., Srivastava, A.K., Rastogi, A., Soni, V.K., 2021. Revisiting Andhi in northern India: a case study of severe dust-storm over the urban megacity of New Delhi. *Urban Clim.* 37, 100825. <https://doi.org/10.1016/j.uclim.2021.100825>.
- Che, H., Wang, Y., Sun, J., Zhang, X., Zhang, X., Guo, J., 2013. Variation of Aerosol Optical Properties over the Taklimakan Desert in China. *Aerosol Air Qual. Res.* 13, 777–785. <https://doi.org/10.4209/aaqr.2012.07.0200>.
- Che, H., Xia, X., Zhao, H., Dubovik, O., Holben, B.N., Goloub, P., Cuevas-Agulló, E., Estelles, V., Wang, Y., Zhu, J., Qi, B., Gong, W., Yang, H., Zhang, R., Yang, L., Chen, J., Wang, H., Zheng, Y., Gui, K., Zhang, X., Zhang, X., 2019. Spatial distribution of aerosol microphysical and optical properties and direct radiative effect from the China Aerosol Remote Sensing Network. *Atmos. Chem. Phys.* 19, 11843–11864. <https://doi.org/10.5194/acp-19-11843-2019>.
- Chen, S., Huang, J., Kang, L., Wang, H., Ma, X., He, Y., Yuan, T., Yang, B., Huang, Z., Zhang, G., 2017. Emission, transport, and radiative effects of mineral dust from the Taklimakan and Gobi deserts: comparison of measurements and model results. *Atmos. Chem. Phys.* 17, 2401–2421. <https://doi.org/10.5194/acp-17-2401-2017>.
- Chen, Y., An, J., Qu, Y., Xie, F., Ma, S., 2023a. Dust radiation effect on the weather and dust transport over the Taklimakan Desert, China. *Atmos. Res.* 284, 106600. <https://doi.org/10.1016/j.atmosres.2022.106600>.
- Chen, Y., Chen, S., Zhou, J., Zhao, D., Bi, H., Zhang, Y., Alam, K., Yu, H., Yang, Y., Chen, J., 2023b. A super dust storm enhanced by radiative feedback. *npj Clim. Atmosph. Sci.* 6, 90. <https://doi.org/10.1038/s41612-023-00418-y>.
- Chooabari, O.A., Zavar-Reza, P., Sturman, A., 2014. The global distribution of mineral dust and its impacts on the climate system: a review. *Atmos. Res.* 138, 152–165. <https://doi.org/10.1016/j.atmosres.2013.11.007>.
- Dong, Q., Huang, Z., Li, W., Li, Z., Song, X., Liu, W., Wang, T., Bi, J., Shi, J., 2022. Polarization Lidar Measurements of Dust Optical Properties at the Junction of the Taklimakan Desert–Tibetan Plateau. *Remote Sens.* 14, 558. <https://doi.org/10.3390/rs14030558>.
- Filonchik, M., 2022. Characteristics of the severe March 2021 Gobi Desert dust storm and its impact on air pollution in China. *Chemosphere* 287 (Part 3), 132219. <https://doi.org/10.1016/j.chemosphere.2021.132219>.
- Gao, J., Ding, T., Gao, H., 2024. Dominant circulation pattern and moving path of the Mongolian Cyclone for the severe sand and dust storm in China. *Atmos. Res.* 301, 107272. <https://doi.org/10.1016/j.atmosres.2024.107272>.
- Goudie, A.S., 2014. Desert dust and human health disorders. *Environ. Int.* 63, 101–113. <https://doi.org/10.1016/j.envint.2013.10.011>.
- Guan, Q., Cai, A., Wang, F., Yang, L., Xu, C., Liu, Z., 2017. Spatio-temporal variability of particulate matter in the key part of Gansu Province, Western China. *Environ. Pollut.* 230, 189–198. <https://doi.org/10.1016/j.envpol.2017.06.045>.
- Han, Y., Wu, Y., Wang, T., Xie, C., Zhao, K., Zhuang, B., Li, S., 2015. Characterizing a persistent Asian dust transport event: Optical properties and impact on air quality through the ground-based and satellite measurements over Nanjing, China. *Atmos. Environ.* 115, 304–316. <https://doi.org/10.1016/j.atmosenv.2015.05.048>.
- Hu, Z., Huang, J., Zhao, C., Bi, J., Jin, Q., Qian, Y., Leung, L.R., Feng, T., Chen, S., Ma, J., 2019. Modeling the contributions of Northern Hemisphere dust sources to dust outflow from East Asia. *Atmos. Environ.* 202, 234–243. <https://doi.org/10.1016/j.atmosenv.2019.01.022>.
- Hu, Q., Wang, H., Goloub, P., Li, Z., Veselovskii, I., Podvin, T., Li, K., Korenskiy, M., 2020a. The characterization of Taklimakan dust properties using a multiwavelength Raman polarization lidar in Kashi, China. *Atmos. Chem. Phys.* 20, 13817–13834. <https://doi.org/10.5194/acp-20-13817-2020>.
- Hu, Z., Huang, J., Zhao, C., Jin, Q., Ma, Y., Yang, B., 2020b. Modeling dust sources, transport, and radiative effects at different altitudes over the Tibetan Plateau. *Atmos. Chem. Phys.* 20, 1507–1529. <https://doi.org/10.5194/acp-20-1507-2020>.
- Hu, Z., Ma, Y., Jin, Q., Idrissa, N.F., Huang, J., Dong, W., 2023. Attribution of the March 2021 exceptional dust storm in North China. *Bull. Am. Meteorol. Soc.* 104 (4), E749–E755. <https://doi.org/10.1175/BAMS-D-22-0151.1>.
- Huang, J., Wang, T., Wang, W., Li, Z., Yan, H., 2014. Climate effects of dust aerosols over East Asian arid and semiarid regions. *J. Geophys. Res. Atmos.* 119, 11,398–11,416. <https://doi.org/10.1002/2014JD021796>.
- Jayarathne, E.R., Johnson, G.R., McGarry, P., Cheung, H.C., Morawska, L., 2011. Characteristics of airborne ultrafine and coarse particles during the Australian dust storm of 23 September 2009. *Atmos. Environ.* 45 (24), 3996–4001. <https://doi.org/10.1016/j.atmosenv.2011.04.059>.
- Ji, Z., Kang, S., Zhang, Q., Cong, Z., Chen, P., Sillanpää, M., 2016. Investigation of mineral aerosols radiative effects over High Mountain Asia in 1990–2009 using a regional climate model. *Atmos. Res.* 178–179, 484–496. <https://doi.org/10.1016/j.atmosres.2016.05.003>.
- Jin, L., He, Q., Jiang, H., Xiao, J., Zhao, Q., Zhou, S., Li, Z., Zhao, J., 2020. Unmanned Aerial Vehicle Observations of the Vertical distribution of Particulate Matter in the Surface Layer of the Taklimakan Desert in China. *Atmosphere* 11, 980. <https://doi.org/10.3390/atmos11090980>.
- Jin, L., He, Q., Li, Z., Deng, M., Abbas, A., 2024. Variation characteristics of dust in the Taklimakan Desert. *Nat. Hazards* 120, 2129–2153. <https://doi.org/10.1007/s11069-023-02626-3>.
- Karydis, V.A., Kumar, P., Barahona, D., Sokolik, I.N., Nenes, A., 2011. On the effect of dust particles on global cloud condensation nuclei and cloud droplet number. *J. Geophys. Res. Atmos.* 116, D23204. <https://doi.org/10.1029/2011JD016283>.
- Kok, J.F., Storelvmo, T., Karydis, V.A., Adebisi, A.A., Mahowald, N.M., Evan, A.T., He, C., Leung, D.M., 2023. Mineral dust aerosol impacts on global climate and climate change. *Nat. Rev. Earth & Environ.* 4, 71–86. <https://doi.org/10.1038/s43017-022-00379-5>.
- Krasnov, H., Katra, I., Koutrakis, P., Friger, M.D., 2014. Contribution of dust storms to PM<sub>10</sub> levels in an urban arid environment. *J. Air Waste Manage. Assoc.* 64, 89–94. <https://doi.org/10.1080/10962247.2013.841599>.
- Li, J., Wang, S., Chu, J., Wang, J., Li, X., Yue, M., Shang, K., 2018. Characteristics of air pollution events over Hotan Prefecture at the southwestern edge of Taklimakan Desert, China. *J. Arid. Land* 10, 686–700. <https://doi.org/10.1007/s40333-018-0096-9>.
- Liu, X., Yin, Z.-Y., Zhang, X., Yang, X., 2004. Analyses of the spring dust storm frequency of northern China in relation to antecedent and concurrent wind, precipitation, vegetation, and soil moisture conditions. *J. Geophys. Res. Atmos.* 109, D16210. <https://doi.org/10.1029/2004JD004615>.
- Liu, Z., Barlow, J.F., Chan, P.-W., Fung, J.C.H., Li, Y., Ren, C., Mak, H.W.L., Ng, E., 2019. A Review of Progress and applications of Pulsed Doppler Wind LiDARs. *Remote Sens.* 11, 2522. <https://doi.org/10.3390/rs11212522>.
- Liu, Y., Wang, G., Hu, Z., Shi, P., Lyu, Y., Zhang, G., Gu, Y., Liu, Y., Hong, C., Guo, L., Hu, X., Yang, Y., Zhang, X., Zheng, H., Liu, L., 2020. Dust storm susceptibility on different land surface types in arid and semiarid regions of northern China. *Atmos. Res.* 243, 105031. <https://doi.org/10.1016/j.atmosres.2020.105031>.

- Mehta, M., Singh, N., Anshumali, 2018. Global trends of columnar and vertically distributed properties of aerosols with emphasis on dust, polluted dust and smoke - inferences from 10-year long CALIOP observations. *Remote Sens. Environ.* 208, 120–132. <https://doi.org/10.1016/j.rse.2018.02.017>.
- Meng, L., Yang, X., Zhao, T., He, Q., Mamtimin, A., Wang, M., Huo, W., Yang, F., Zhou, C., Pan, H., 2020. Simulated regional transport structures and budgets of dust aerosols during a typical springtime dust storm in the Tarim Basin, Northwest China. *Atmos. Res.* 238, 104892 <https://doi.org/10.1016/j.atmosres.2020.104892>.
- Merdji, A., Lu, C., Xu, X., Mhawish, A., 2023. Long-term three-dimensional distribution and transport of Saharan dust: Observation from CALIPSO, MODIS, and reanalysis data. *Atmos. Res.* 286, 106658 <https://doi.org/10.1016/j.atmosres.2023.106658>.
- Mu, L., Su, J., Mo, X., Peng, N., Xu, Y., Wang, M., Wang, J., 2021. The Temporal-Spatial Variations and potential Causes of Dust events in Xinjiang Basin during 1960–2015. *Front. Environ. Sci.* 9, 727844 <https://doi.org/10.3389/fenvs.2021.727844>.
- Pu, B., Jin, Q., 2021. A record-breaking trans-Atlantic African dust plume associated with atmospheric circulation extremes in June 2020. *Bull. Am. Meteorol. Soc.* 102 (7), E1340–E1356. <https://doi.org/10.1175/BAMS-D-21-0014.1>.
- Qian, Y., Yasunari, T.J., Doherty, S.J., Flanner, M.G., Lau, W.K.M., Ming, J., Wang, H., Wang, M., Warren, S.G., Zhang, R., 2015. Light-absorbing particles in snow and ice: Measurement and modeling of climatic and hydrological impact. *Adv. Atmos. Sci.* 32, 64–91. <https://doi.org/10.1007/s00376-014-0010-0>.
- Sun, X., Fan, X., Zhang, T., Wang, Y., Wang, Y., Lyu, D., Zheng, M., 2022. Tempo-Spatial Distributions and Transport Characteristics of two Dust events over Northern China in March 2021. *Remote Sens.* 14, 5967. <https://doi.org/10.3390/rs14235967>.
- Tam, W.W.S., Wong, T.W., Wong, A.H.S., Hui, D.S.C., 2012. Effect of dust storm events on daily emergency admissions for respiratory diseases. *Respirology* 17, 143–148. <https://doi.org/10.1111/j.1440-1843.2011.02056.x>.
- Tang, D., Wei, T., Yuan, J., Xia, H., Dou, X., 2022. Observation of bioaerosol transport using wideband integrated bioaerosol sensor and coherent Doppler lidar. *Atmos. Meas. Tech.* 15, 2819–2838. <https://doi.org/10.5194/amt-15-2819-2022>.
- Tao, M., Gui, L., Li, R., Wang, L., Liang, S., Li, Q., Wang, L., Yu, C., Chen, L., 2021. Tracking prevailing dust aerosol over the air pollution in Central China with integrated satellite and ground observations. *Atmos. Environ.* 253, 118369 <https://doi.org/10.1016/j.atmosenv.2021.118369>.
- Uno, I., Eguchi, K., Yumimoto, K., Takemura, T., Shimizu, A., Uematsu, M., Liu, Z., Wang, Z., Hara, Y., Sugimoto, N., 2009. Asian dust transported one full circuit around the globe. *Nat. Geosci.* 2, 557–560. <https://doi.org/10.1038/ngeo583>.
- Victor, J.N., Potdar, S.S., Siingh, D., Gokul, T., Kamra, A.K., Singh, R.P., Gopalakrishnan, V., Pandithurai, G., 2024. Impact of a severe dust storm on aerosol properties and their radiative forcing over the Indian subcontinent during winter. *Atmos. Res.* 301, 107282 <https://doi.org/10.1016/j.atmosres.2024.107282>.
- Wang, S., Yuan, W., Shang, K., 2006. The impacts of different kinds of dust events on PM10 pollution in northern China. *Atmos. Environ.* 40 (40), 7975–7982. <https://doi.org/10.1016/j.atmosenv.2006.06.058>.
- Wu, C., Lin, Z., Shao, Y., Liu, X., Li, Y., 2022. Drivers of recent decline in dust activity over East Asia. *Nat. Commun.* 13, 7105. <https://doi.org/10.1038/s41467-022-34823-3>.
- Xiao, F., Zhou, C., Liao, Y., 2008. Dust storms evolution in Taklimakan Desert and its correlation with climatic parameters. *J. Geogr. Sci.* 18, 415–424. <https://doi.org/10.1007/s11442-008-0415-8>.
- Xie, S., Yu, T., Zhang, Y., Zeng, L., Qi, L., Tang, X., 2005. Characteristics of PM10, SO2, NOx and O3 in ambient air during the dust storm period in Beijing. *Sci. Total Environ.* 345 (1–3), 153–164. <https://doi.org/10.1016/j.scitotenv.2004.10.013>.
- Xiong, Z., Xu, X., Yang, Y., Luo, T., 2023. Diurnal vertical distribution and transport of dust aerosol over and around Tibetan Plateau from lidar on International Space Station. *Atmos. Res.* 294, 106939 <https://doi.org/10.1016/j.atmosres.2023.106939>.
- Xu, X., Wu, H., Yang, X., Xie, L., 2020. Distribution and transport characteristics of dust aerosol over Tibetan Plateau and Taklimakan Desert in China using MERRA-2 and CALIPSO data. *Atmos. Environ.* 237, 117670 <https://doi.org/10.1016/j.atmosenv.2020.117670>.
- Yang, X., Shen, S., Yang, F., He, Q., Ali, M., Huo, W., Liu, X., 2016. Spatial and temporal variations of blowing dust events in the Taklimakan Desert. *Theor. Appl. Climatol.* 125, 669–677. <https://doi.org/10.1007/s00704-015-1537-4>.
- Yu, T., Xiaole, P., Yujie, J., Yuting, Z., Weijie, Y., Hang, L., Shandong, L., Zifa, W., 2023. East Asia dust storms in spring 2021: Transport mechanisms and impacts on China. *Atmos. Res.* 290, 106773 <https://doi.org/10.1016/j.atmosres.2023.106773>.
- Zhang, B., Tsunekawa, A., Tsubo, M., 2008. Contributions of sandy lands and stony deserts to long-distance dust emission in China and Mongolia during 2000–2006. *Glob. Planet. Chang.* 60 (3–4), 487–504. <https://doi.org/10.1016/j.gloplacha.2007.06.001>.
- Zhou, C., Liu, Y., He, Q., Zhong, X., Zhu, Q., Yang, F., Huo, W., Mamtimin, A., Yang, X., Wang, Y., Meng, L., 2022. Dust Characteristics Observed by Unmanned Aerial Vehicle over the Taklimakan Desert. *Remote Sens.* 14, 990. <https://doi.org/10.3390/rs14040990>.
- Zhou, Y., Gao, X., Lei, J., 2023. Characteristics of Dust Weather in the Tarim Basin from 1989 to 2021 and its Impact on the Atmospheric Environment. *Remote Sens.* 15, 1804. <https://doi.org/10.3390/rs15071804>.